DOI: 10.1002/ejic.201000610

Structure–Property Relationship of Red- and Green-Emitting Iridium(III) Complexes with Respect to Their Temperature and Oxygen Sensitivity

Nan Tian,[a,b] Daniel Lenkeit,[a] Simon Pelz,[a] Lorenz H. Fischer,[c] Daniel Escudero,*[d] Ralf Schiewek,[e] Dennis Klink,[e] Oliver J. Schmitz,[e] Leticia González,[d] Michael Schäferling,*[c] and Elisabeth Holder*[a,b]

Keywords: Iridium / Phosphorescence / Temperature sensitivity / Oxygen sensitivity / Density functional calculations

We report on the structural design and characterization of a series of neutral heteroleptic iridium(III) complexes equipped with 2-phenylpyridine, 2-(naphthalen-1-yl)pyridine, and 1-phenylisoquinoline as cyclometalating ligands. To gradually increase the unsymmetrical architecture of the heteroleptic iridium(III) complexes, they have been furnished with 2,2,6,6-tetramethylheptane-3,5-dione, 1-(9*H*-carbazol-9-yl)-5,5-dimethylhexane-2,4-dione, and 1-[3,6-bis(4-hexylphenyl)-9*H*-carbazol-9-yl]-5,5-dimethylhexane-2,4-dione as ancillary ligands. The photophysical and electrochemical properties of these asymmetric Ir^{III} complexes have been investigated experimentally as well as theoretically by using density functional theory (DFT) calculations. The properties of these new neutral heteroleptic iridium(III) complexes have been experimentally compared to homoleptic Ir^{III} complex structures that reveal symmetrical architectures due to three similar cyclometalating ligands. The emission intensity of the herein described two classes of Ir^{III} complexes is clearly influenced by applying changes to temperature and air pressure. The emphasis is on general design rules for oxygen-sensitive Ir^{III} emitters due to the correlation of the structure-dependent oxygen sensitivity to their phosphorescence lifetimes.

Introduction

Neutral iridium(III) complexes received much attention due to their outstanding optical properties,[1–6] which make them highly valuable in light-emitting diodes[7] or sensor systems[8] as well as in biomedical imaging.[9] On account of the extraordinary possibility to intermix excited states, they usually reveal intensive and, due to spin–orbit coupling, spin-allowed phosphorescence in both solution and bulk.[1,4] The intermixed states, namely, singlet and triplet metal-to-ligand charge-transfer (MLCT) states as well as singlet and triplet ligand-centered (LC) states[10] allow the variation of the phosphorescence emission[11,12] from blue[13] to near-infrared[14] by the structural design of Ir^{III} complexes. Besides the color variation on demand, neutral cyclometalated Ir^{III} complexes are furnished with high photostability and quantum yields[3,4] as well as lifetimes of usually several microseconds.[10] The lowest triplet MLCT states[15] have to be controlled to tailor the phosphorescence of iridium(III) complexes.[11,12] All phosphorescent light emission occurs from these states. A series of design rules have to be obeyed to obtain Ir^{III} complexes that can be easily pumped and show efficient emission, microsecond lifetimes, high complex stability, and sensitivity to their environment:[11,12] (1) The lowest excited state must be of charge-transfer (CT) or of intraligand (IL) π–π* character to prevent photochemical instability. (2) Metal-centered (MC) d–d excited states must be above the emitting level; this helps to prevent thermal excitation that leads to efficient excited state decay and thus to photochemical instability. (3) Spin–orbit coupling should be high to enhance radiative decay (S_n and T_n), thereby competing with radiationless decay (T_1 and S_0). (4) Pure π–π* phosphorescence has a tendency to be long-lived, hence preventing efficient emission; thus, either spin–orbit coupling or mixing with CT states is required to effectively increase π–π* phosphorescence. (5) The emitting state should not be too low in energy, because low-lying emitting states enhance radiationless processes.

In addition to the above-mentioned precious optical properties and general design rules,[11,12] the phosphorescence of different neutral Ir^{III} complexes is sensitive

[a] Functional Polymers Group and Institute of Polymer Technology, University of Wuppertal,
Gaußstr. 20, 42097 Wuppertal, Germany
Fax: +49-202-439-3880
E-mail: holder@uni-wuppertal.de
[b] Dutch Polymer Institute (DPI),
P. O. Box 513, 5600 AX Eindhoven, The Netherlands
[c] Institute of Analytical Chemistry, Chemo- and Biosensors, University of Regensburg,
93040 Regensburg, Germany
Fax: +49-941-943-4064
E-mail: michael.schaeferling@chemie.uni-regensburg.de
[d] Institute of Physical Chemistry,
Friedrich Schiller University Jena,
Helmholtzweg 4, 07743 Jena, Germany
Fax: +49-3641-948302
E-mail: daniel.escudero@uni-jena.de
[e] Analytical Chemistry, University of Wuppertal,
Gaußstr. 20, 42097 Wuppertal, Germany
Supporting information for this article is available on the WWW under http://dx.doi.org/10.1002/ejic.201000610.

towards oxygen (and therefore to barometric pressure) and temperature.[8,16,17] Luminescent oxygen- and temperature-sensitive probes have found numerous applications in optical sensors, biomedical imaging, and pressure- or temperature-sensitive paints for fluid mechanics. Neutral iridium(III) complexes can be commonly divided into structures of homoleptic and heteroleptic architecture.[7,12] Generally, unsymmetrical structures (in the case of Ir^{III} emitters, heteroleptic architectures) induce high environmental sensitivity.

Temperature sensitivity can be achieved by having two states of different nature within an energy gap of kT of each other. Applying temperature will then change the population of the quasidegenerate states and thus influence the decay rates, emission intensities, and lifetimes. One option is the thermal activation of an MC state; conversely, care must be taken to not induce permanent decomposition.[11]

To achieve oxygen sensitivity based on phosphorescence quenching, one has to focus on structures with high quantum yields and long lifetimes.[16,18] However, within a given class of complexes the bimolecular rate constants are insensitive to the specific structure.[11] This rule also applies to pressure sensitivity, as shown in the present investigation.

In this study, we report on the synthesis and characterization of a series of heteroleptic green, orange-red, and red Ir^{III} complexes that were carefully designed by applying the above-mentioned rules. DFT and time-dependent DFT (TD-DFT) studies of the ground and excited states of selected Ir^{III} complexes have been performed to help interpret the experimental photophysical data. Moreover, the characteristics of these novel heteroleptic complexes have been compared to a selection of already known homoleptic Ir^{III} complexes based on cyclometalating C^N-type ligands of blue, green, and red emission color. It was attempted to reveal a general synthetic design concept to obtain iridium(III) complexes with a pronounced sensitivity to oxygen (and likewise air pressure) or temperature.

Results and Discussion

Synthesis and Characterization

To study the oxygen (in terms of barometric pressure) and temperature sensitivity of a selection of blue-, green-, and red-emitting homoleptic and heteroleptic iridium(III) complexes, a series of unsymmetrical heteroleptic phosphorescent green, orange-red, and red iridium(III) complexes were synthesized and characterized. For this purpose, a set of C^N and ancillary ligands were prepared.[7] 1-Phenylisoquinoline (**1**)[7] (see Supporting Information) was obtained by an optimized and simplified Suzuki protocol[19] in 92% yield by using tetrakis(triphenylphosphane)palladium(0) as cross-coupling catalyst.

The same (but intensively optimized) reaction pathway was used to couple (4-hexylphenyl)boronic acid (**2**) (see Figure S1) with 3,6-diiodo-9*H*-carbazole[20,21] to yield novel 3,6-bis(4-hexylphenyl)-9*H*-carbazole (**3**) (see Figure S1) in 58% yield. Tetrakis(triphenylphosphane)palladium(0) was yet again utilized as cross-coupling catalyst (Figure S1 in the Supporting Information). Several attempts of using modified Suzuki C–C coupling protocols were carried out to obtain compound **3**. However, reactions performed by using other cross-coupling functionalities like bromo functions, that were combined with a series of boronic acid esters, ended only in no or low conversion with unsatisfactory yields of **3**. This finding goes hand-in-hand with rarely described reactions of the same type in the literature.[22] Only a few examples can be found of coupling bare phenyl substituents onto carbazoles in their 3,6-position.[22,23] Ethyl 2-[3,6-bis(4-hexylphenyl)-9*H*-carbazol-9-yl]acetate (**4**) (see Figure S1) was obtained in a yield of 62% by treating **3** with ethyl 2-bromoacetate under K_2CO_3 basic conditions.[8,24] Subsequently, 1-[3,6-bis(4-hexylphenyl)-9*H*-carbazol-9-yl]-5,5-dimethylhexane-2,4-dione (**5**) (see Figure S1) was obtained in a yield of 80% by treating **4** with 3,3-dimethyl-2-oxobutan-1-ide, which was obtained by using potassium hexamethyldisilazane (KHMDS), in a Claisen-type reaction.[8,24] The μ-chlorido-bridged dimers **6a**–**c** (see Supporting Information) were synthesized in yields of 70–78% according to the well-known Nonoyama method,[25] but treating $IrCl_3 \cdot nH_2O$ with **1** (1-phenylisoquinoline, piq), 2-(naphthalen-1-yl)pyridine (npy), and 2-phenylpyridine (ppy), respectively. Heteroleptic iridium(III) complexes **7a**–**c** were prepared in yields of 66–71% by combining **6a**–**c** with commercially available 2,2,6,6-tetramethylheptane-3,5-dione (denoted as acac) according to a bridge-splitting method using K_2CO_3 as base (Figure 1). Iridium(III) complexes **8a**–**c** (Figure 1) were obtained in yields of 61–67% according to the same reaction conditions but by treating **6a**–**c** with 1-(9*H*-carbazol-9-yl)-5,5-dimethylhexane-2,4-dione (denoted as carbazole–acac).[8] Finally, the iridium(III) complexes **9a**–**c** (yield: 65–72%) were obtained by adding 1-[3,6-bis(4-hexylphenyl)-9*H*-carbazol-9-yl]-5,5-dimethylhexane-2,4-dione (denoted as phenyl–carbazole–acac) to **6a**–**c** (Figure 1). The complexes in the series **7a**–**c** to **9a**–**c** were easily soluble in solvents of medium polarity.

^1H NMR spectra were obtained from solutions of the compounds in deuterated chloroform. The structures of **7a**–**c** to **9a**–**c** were confirmed by applying 2D ^1H–^1H COSY NMR spectroscopic experiments. Atmospheric-pressure laser-ionization mass-spectrometry (APLI-MS) techniques were additionally utilized to identify the molecular weight and the purity of the heteroleptic Ir^{III} complexes **7a**–**c** to **9a**–**c**. For all heteroleptic complexes **7a**–**c** to **9a**–**c** the molecular peak could be detected according to the calculated values and, moreover, the molecular-peak pattern could be exactly simulated. In addition, correct elemental analyses proved the purity of compounds **7a**–**c** to **9a**–**c**, correspondingly. All of the heteroleptic Ir^{III} complexes **7a**–**c** to **9a**–**c** were subjected to thermal gravimetric analysis (TGA) to verify that their thermal stability was higher than 280 °C at 5% weight loss, thus qualifying the novel compounds **7a**–**c** to **9a**–**c** as probes with excellent temperature stabilities (Table 1).

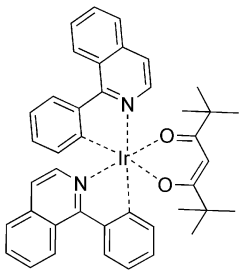

7a

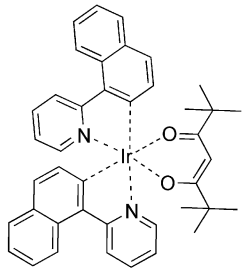

7b

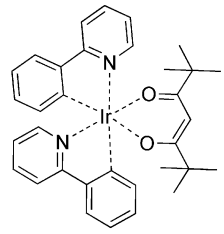

7c

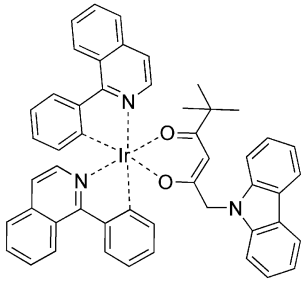

8a

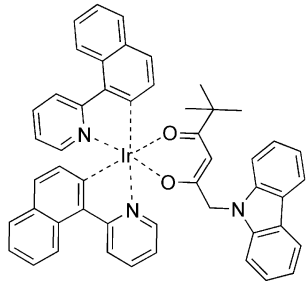

8b

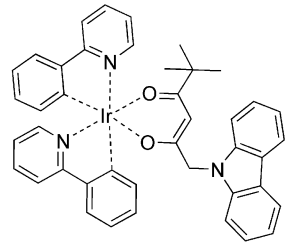

8c

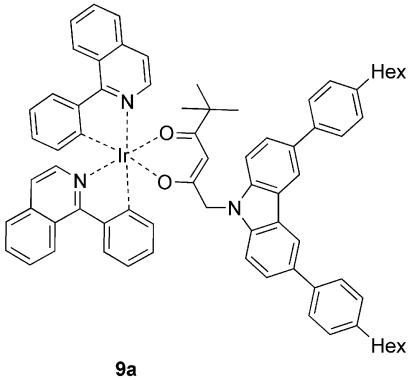

9a

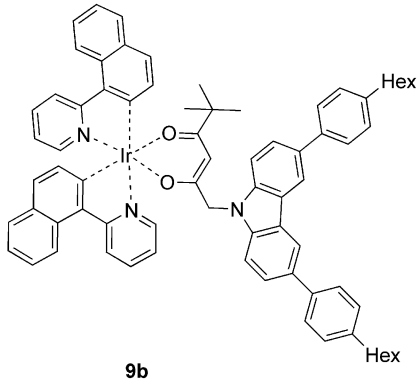

9b

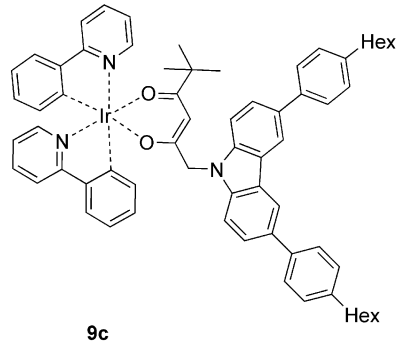

9c

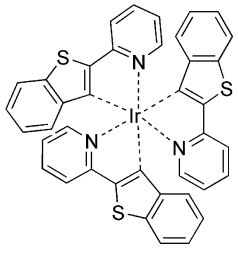

10

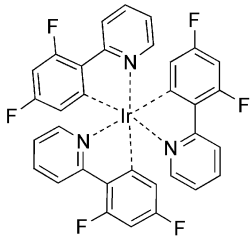

11

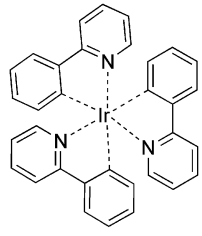

12

Figure 1. Schematic representation of the structures of the analyzed heteroleptic complexes **7a**–**c** to **9a**–**c** and homoleptic Ir^{III} complexes **10**–**12**.

Table 1. Data of absorption, emission, quantum yields, and decomposition temperature (T_d) for iridium(III) complexes.

Material	Absorbance [nm] ($\log\varepsilon$ [$L\,mol^{-1}\,cm^{-1}$])	Maximum emission [nm]	Quantum yield[a] [%]	T_d[b] [°C]
7a	293 (4.98), 344 (3.73) 419 (3.28), 484 (3.20)	630	35	284.3
7b	240 (4.03), 300 (4.04) 458 (3.11), 497 (3.14)	600	37	281.2
7c	260 (5.29), 341 (3.62) 412 (3.25), 468 (3.14)	522	43	302.3
8a	247 (5.33), 291 (5.20) 341 (3.93), 478 (3.29)	624	31	356.0
8b	242 (3.99), 296 (3.87) 346 (3.54), 490 (2.83)	597	34	336.0
8c	240 (4.02), 262 (3.99) 345 (3.37), 462 (2.70)	521	37	337.3
9a	264 (3.97), 299 (3.98) 359 (3.40), 481 (2.79)	625	30	340.0
9b	262 (5.06), 296 (5.02) 356 (3.66), 490 (3.18)	595	32	315.6
9c	235 (3.86), 262 (5.08) 291 (3.98), 466 (2.49)	522	44	324.6

[a] Determined according to the method of Demas and Crosby.[28] [b] At 5% weight loss.

Optical Properties

The experimental UV/Vis absorption and emission spectra of complexes **7a**–**c** to **9a**–**c** recorded in $CHCl_3$ are depicted in Figure 2. Table 1 collects their photophysical characteristics. To gain insight into the excited states that are responsible for the photophysical properties of these Ir^{III} complexes, theoretical Δ-DFT and TD-DFT (B3LYP/6-31G*) calculations have been performed, by way of example, for complexes **7a**,**c** and **8a**,**c** (see Figure 1). Figures 3 and 4 show their corresponding Kohn–Sham orbitals and the energy-level schemes. In all the complexes the HOMO orbital is the $5d_{xy}$ orbital of the Ir^{III} center. The rest of the orbitals of the set t_{2g} ($5d_{xz}$ and $5d_{yz}$ orbitals) are found to occupy lower-lying energy levels. In the case of complexes **7a** (Figure 3) and **8c** (Figure 4), some π orbitals localized in the ancillary ligand (π_{anc}) are intercalated within the set t_{2g} of orbitals. Interestingly, for all the complexes the LUMO orbital is a π-antibonding orbital localized on the cyclometalating ligand (π^*_{cycl}).

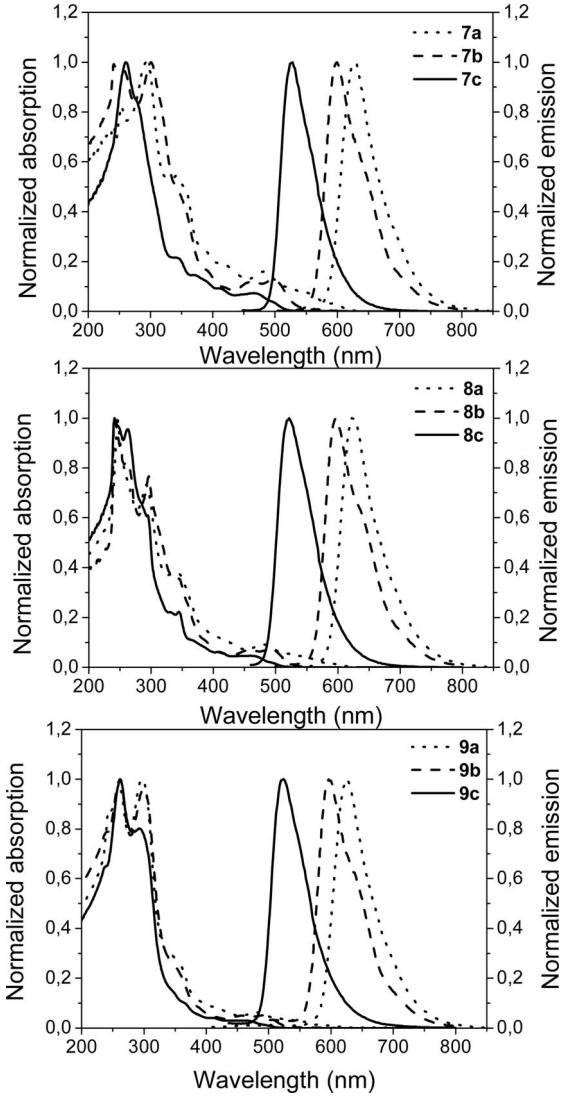

Figure 2. Absorption and emission properties of the iridium(III) complex series **7a**–**c** to **9a**–**c** (10^{-5} M in $CHCl_3$).

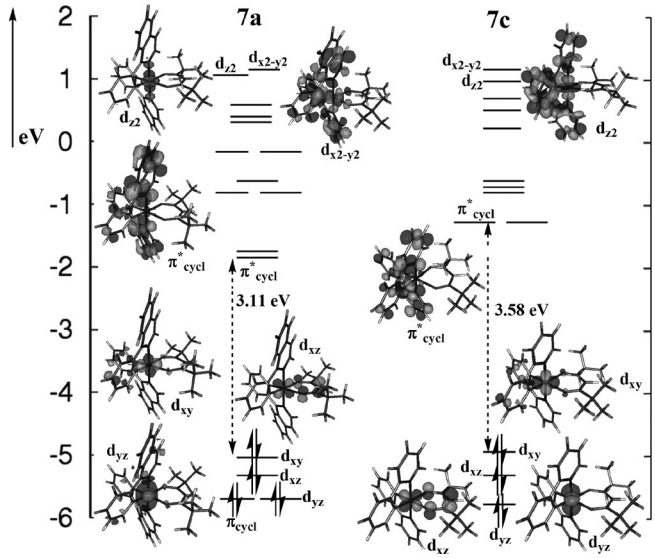

Figure 3. Energy-level scheme of complexes **7a**,**c**, including the most relevant Kohn–Sham orbitals and the HOMO–LUMO gaps calculated with B3LYP/6-31G*.

In the cyclometalating piq-based complexes **7a** and **8a**, the LUMO orbital is stabilized relative to the LUMO orbital of the ppy-based complexes **7c** and **8c**. This stabilization is due to the delocalization of this orbital in the piq cyclometalating ligand relative to the ppy ligand. Since the HOMO energies are very close within the piq/ppy series, larger HOMO–LUMO gaps are obtained for the ppy series (compare 3.58–3.61 eV to 3.11–3.09 eV, in Figures 3 and 4). The e_g orbitals of the Ir^{III} center are, as seen in Figures 3 and 4, strongly destabilized for all the complexes. This is a

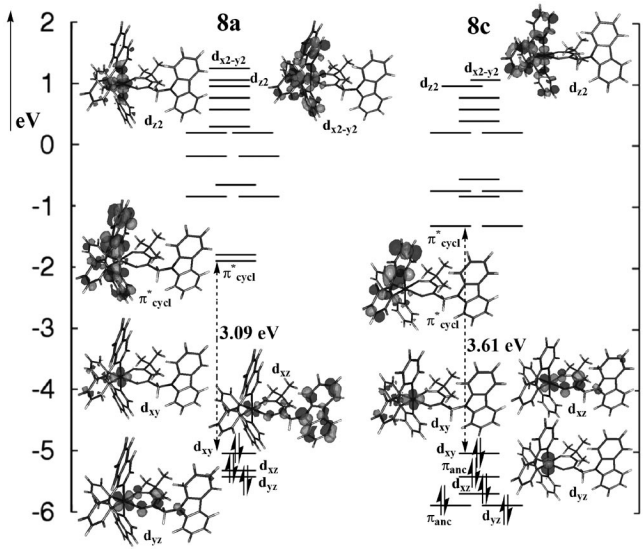

Figure 4. Energy-level scheme of complexes **8a**,**c**, including the most relevant Kohn–Sham orbitals and the HOMO–LUMO gaps calculated with B3LYP/6-31G*.

common feature for cyclometalated Ir^{III} complexes, since the strong ligand-field effect of the phenyl anion (C⁻^N) ligand increases the gap between the sets of t_{2g} and e_g orbitals.

In the following, we turn our attention to the interpretation of the UV/Vis data. The UV/Vis spectra of complexes **7a**–**c** to **9a**–**c** show some general features. The photophysical properties are more robust within the same cyclometalating ligand series rather than with the same ancillary ligand (compare the UV/Vis spectra of complexes with the same ancillary ligand, e.g., **7a** vs. **7c** with respect to complexes with the same cyclometalating ligand, e.g., **7c** vs. **8c**). In the complexes that bear the piq and npy cyclometalating ligands, more common features are obtained than with the ppy cyclometalating ligands. The UV/Vis spectra of all the complexes are dominated by some intense absorption bands located in the far-UV region (below 300 nm). In the piq- and npy-based complexes, these bands are split into two main peaks at 300 and 250 nm. In the ppy-based compounds, a single band peaks at about 260 nm. Some shoulders of the aforementioned intense bands higher in energy (around 350 nm) can be seen in all complexes. Between 450 and 550 nm, low-lying weak absorption bands follow.

A comparison of the calculated and experimental absorption spectra for complexes **7a**,**c** and **8a**,**c** is presented in Figure 5. The associated most relevant electronic singlet–singlet vertical excitations, their oscillator strengths, and their correspondent assignments are summarized in Table 2. Among them, we find ^{1}MLCT states, IL excitations as well as ligand-to-ligand CT excitations (^{1}LLCT). The simulated convoluted UV/Vis spectra are shown in Figure 5 with dashed lines. As can be seen, the agreement between the calculated and experimental spectra is very good, notwithstanding that TD-DFT tends to underestimate CT states.[26] The weak experimental absorption bands located between 450 and 550 nm are theoretically assigned as spin-allowed ^{1}MLCT transitions (see, for example, S_1, S_2, S_3, and S_6 in complex **7a** in Table 2). These electronic excitations are red-shifted for the piq-based complexes, as stated both theoretically and experimentally (see Figure 5). This fact can be explained through the above-mentioned stabilization of the cyclometalating-based antibonding orbitals of the piq-related compounds. As shown in Figure 5, no absorption is predicted beyond 550 nm in complexes **7a**,**c** and beyond 480 nm for complexes **8a**,**c**. The long tails of, for instance, **8a** up to 600 nm, at which point singlet–singlet excitations are dark or do not exist, should then be attributed to ^{3}MLCT excited states.[10,24,27] The very intense bands that peak in the region of 300 nm for complexes **7a** and **8a** and approximately 260 nm for complexes **7c** and **8c** are of very different character. They correspond to high-energy ^{1}MLCT transitions in case of **7a**,**c** (see S_{25} and S_{35} for complexes **7a** and **8a** in Table 2), whereas in **7c** and **8c** they are due to mainly IL π→π* transitions within the cyclometalating ligands (see S_{36} and S_{50} for complexes **7c** and **8c**, respectively). These ligand-based bands are also present but slightly blueshifted in the npy and piq series (peaking at around 250 nm; see Figure 2). As expected, these bands are also present in the UV/Vis spectra of the isolated cyclometalating ligands 2-phenylpyridine, **1**, and 2-(naphthalen-1-yl)pyridine, respectively.[10,24] The β-diketonato-based transitions also contribute to these bands at about 270 nm (see S_{46} and S_{42} for complexes **8a** and **8c**, respectively, in Table 2), which is analogous to the absorptions of the free β-diketone. The shoulders of the intense band located in the visible region at around 300–350 nm in complexes **7c** and **8c** and at approximately 350–400 nm in complexes **7a** and **8a** are due to electronic transitions of a very diverse nature. Among them, ^{1}IL as well as ^{1}MLCT transitions dominate this region.

Next, we shall discuss the nature of the excited states involved in the emission process. The experimental phosphorescence spectra can also be found in Figure 2. Complexes **7a**–**9a** present maximum emission wavelengths (λ_{max}) that are higher than 624 nm as intense red light with quantum yields of more than 30%. The complexes **7b**–**9b** show orange-red phosphorescence ($\lambda_{max} \approx$ 595–600 nm) with quantum yields higher than 32%. Typically, the series of green-emitting ($\lambda_{max} \approx$ 521–522 nm) complexes **7c**–**9c** reveal the uppermost quantum yield of 44% (see Table 1). Since the lowest triplet excited states involve a π* orbital located on the cyclometaling ligand (vide infra), this ligand should play the most important role in the emission spectra, as experimentally confirmed within the series **7a**–**9a**, **7b**–**9b** and **7c**–**9c**.

For Ir^{III} complexes it is well known that the lowest triplet excited state (T_1) is populated rapidly through an efficient intersystem crossing between the manifolds of singlets and triplets (due to strong spin–orbit coupling for the Ir^{III} atom). To reproduce the emission-spectral maxima of **7a**,**c** and **8a**,**c** theoretically, a two-step approach has been considered. First, the five lowest-lying triplet excitations at the Franck–Condon geometry have been obtained at the TD-

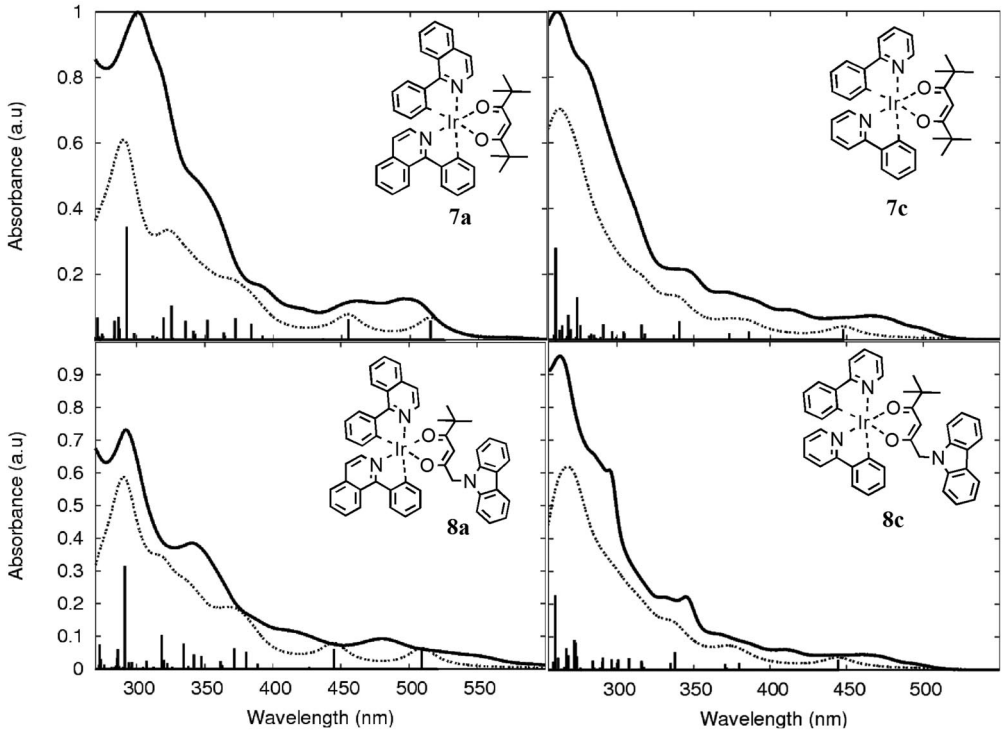

Figure 5. Experimental UV/Vis spectra (solid lines) of complexes **7a**,**c** and **8a**,**c** with TD-DFT (B3LYP/6-31G*) vertical excitations. The simulated UV/Vis spectra with a Lorentzian broadening of 25 nm of band width on half-height are presented with dashed lines.

Table 2. Main theoretical electronic-transition energies (ΔE), with corresponding oscillator strengths (f) and assignments of complexes **7a**,**c** and **8a**,**c**.

State	ΔE [nm]	f	Assignment	State	ΔE [nm]	f	Assignment
		7a				**7c**	
S_1	525	0.001	$5d_{xy}\rightarrow\pi^*_{cycl}$ (0.68) MLCT	S_1	448	0.032	$5d_{xy}\rightarrow\pi^*_{cycl}$ (0.68) MLCT
S_2	515	0.059	$5d_{xy}\rightarrow\pi^*_{cycl}$ (0.68) MLCT	S_3	386	0.025	$5d_{xz}\rightarrow\pi^*_{cycl}$ (0.68) MLCT
S_3	455	0.063	$5d_{xz}\rightarrow\pi^*_{cycl}$ (0.69) MLCT	S_8	341	0.056	$5d_{yz}\rightarrow\pi^*_{cycl}$ (0.66) MLCT
S_6	384	0.049	$5d_{yz}\rightarrow\pi^*_{cycl}$ (0.61) MLCT	S_{14}	316	0.047	$\pi_{cycl}\rightarrow\pi^*_{cycl}$ (0.48) IL
S_7	372	0.066	$\pi_{cycl}\rightarrow\pi^*_{cycl}$ (0.63) IL	S_{19}	291	0.048	$\pi_{cycl}\rightarrow\pi^*_{cycl}$ (0.51) IL
S_{12}	352	0.060	$\pi_{cycl}\rightarrow\pi^*_{cycl}$ (0.68) IL	S_{27}	276	0.045	$\pi_{anc}\rightarrow\pi^*_{cycl}$ (0.47) LLCT
S_{18}	326	0.105	$d_{xz}\rightarrow\pi^*_{cycl}$ (0.53) MLCT	S_{28}	274	0.130	$\pi_{anc}\rightarrow\pi^*_{cycl}$ (0.48) LLCT
S_{19}	320	0.068	$4d_{xz}\rightarrow\pi^*_{cycl}$ (0.53) MLCT	S_{31}	268	0.076	$\pi_{anc}\rightarrow\pi^*_{cycl}$ (0.38) LLCT
S_{25}	293	0.344	$5d_{xz}\rightarrow\pi^*_{cycl}$ (0.61) MLCT	S_{34}	264	0.044	$\pi_{cycl}\rightarrow\pi^*_{cycl}$ (0.52) IL
S_{28}	287	0.070	$\pi_{cycl}\rightarrow\pi^*_{cycl}$ (0.54) IL	S_{36}	260	0.275	$\pi_{cycl}\rightarrow\pi^*_{cycl}$ (0.39) IL
		8a				**8c**	
S_1	521	0.001	$5d_{xy}\rightarrow\pi^*_{cycl}$ (0.68) MLCT	S_1	444	0.030	$5d_{xy}\rightarrow\pi^*_{cycl}$ (0.68) MLCT
S_2	509	0.056	$5d_{xy}\rightarrow\pi^*_{cycl}$ (0.68) MLCT	S_3	380	0.022	$5d_{xz}\rightarrow\pi^*_{cycl}$ (0.57) MLCT
S_3	445	0.062	$5d_{yz}\rightarrow\pi^*_{cycl}$ (0.62) MLCT	S_{10}	338	0.055	$5d_{yz}\rightarrow\pi^*_{cycl}$ (0.58) MLCT
S_8	381	0.053	$4d_{xz}\rightarrow\pi^*_{cycl}$ (0.59) MLCT	S_{22}	308	0.035	$\pi_{anc}\rightarrow\pi^*_{anc}$ (0.60) IL
S_9	372	0.062	$\pi_{cycl}\rightarrow\pi^*_{cycl}$ (0.57) IL	S_{28}	291	0.037	$\pi_{cycl}\rightarrow\pi^*_{cycl}$ (0.43) IL
S_{17}	342	0.043	$4d_{yz}\rightarrow\pi^*_{cycl}$ (0.60) MLCT	S_{40}	274	0.042	$\pi_{anc}\rightarrow\pi^*_{cycl}$ (0.37) LLCT
S_{19}	334	0.077	$\pi_{cycl}\rightarrow\pi^*_{cycl}$ (0.57) IL	S_{42}	273	0.082	$\pi_{anc}\rightarrow\pi^*_{anc}$ (0.37) IL; $\pi_{cycl}\rightarrow\pi^*_{cycl}$ (–0.38) IL
S_{24}	319	0.105	$\pi_{cycl}\rightarrow\pi^*_{cycl}$ (0.42) IL	S_{44}	272	0.090	$\pi_{cycl}\rightarrow\pi^*_{cycl}$ (0.31) IL
S_{35}	291	0.315	$4d_{xz}\rightarrow\pi^*_{cycl}$ (0.59) MLCT	S_{46}	267	0.065	$5d_{yz}\rightarrow\pi^*_{cycl}$ (0.32) MLCT
S_{46}	274	0.075	$\pi_{anc}\rightarrow\pi^*_{anc}$ (0.54) IL	S_{50}	260	0.227	$\pi_{cycl}\rightarrow\pi^*_{cycl}$ (0.31) IL

B3LYP/6-31G* level of theory (see Table 3). All of them are of ^{3}MLCT character. The so-obtained S_0–T_1 gaps are clearly blueshifted with respect to the experimental emission maxima. This is expected since the triplet states have not been allowed to relax. Therefore, as a second step, triplet-state optimizations were carried out to yield adiabatic emission energies (*AEE*; see Table 3). We note that relaxation along the triplet potential-energy surfaces leads to the same triplet excited state regardless of substitution of the ancillary or cyclometalating ligands. Thus, the T_1 minima

Table 3. Lowest singlet–triplet theoretical emission energies by means of TD-DFT and Δ-DFT approaches.

	7a	**7c**	**8a**	**8c**
	TD-DFT vertical singlet–triplet excitations; ΔE [nm] and resulting ^{3}MLCT assignment			
T_1	592	490	592	486
T_2	585	478	581	480
T_3	512	427	504	430
T_4	506	416	501	414
T_5	452	413	445	412
	Theoretical E_{e-e}; ΔE [nm] (experimental E_{0-0} [nm])			
	615 (545)	500 (489)	610 (572)	499 (479)
	Theoretical *AEE*; ΔE [nm] (experimental emission maxima [nm])			
	701 (630)	550 (522)	698 (624)	548 (521)

of all the complexes are of ^{3}MLCT character, as reflected through the analysis of spin densities and in accordance to the TD-DFT data. They are all transitions going from a d orbital of the Ir^{III} atom to a π^*_{cycl} orbital. As it can be seen in Table 3, the *AEE* values (obtained as the energy difference between T_1 and S_0 at the optimized T_1 geometry) are then in more reasonable agreement with the experimental emission maxima (errors amount to 0.2 eV, which is the accepted error inherent to the functional). The theoretical values of 701, 550, 698, and 548 nm, obtained for **7a**, **7c**, **8a**, and **8c**, respectively, correlate well with the experimental ones of 630, 522, 624, and 521 nm (Table 3). The electronic ZPE E_{e-e} energies (i.e., the energy difference between T_1 and S_0 minima on each potential-energy surface) also show a fair agreement with the E_{0-0} experimental values (estimated experimentally as the intersection point between the emission and absorption spectra).

Pressure and Temperature Sensitivity

The pressure (pO_2) and temperature dependency of the phosphorescence lifetimes of compounds **7a**–**c**, **8b**–**c**, **9b**–**c**, and of three commercially available homoleptic iridium(III) complexes {tris[2-(benzo[*b*]thiophen-2-yl)pyridinato-C^3,*N*]-iridium(III), [Ir(btpy)$_3$] (**10**); tris[2-(4,6-difluorophenyl)-pyridinato-C^2,*N*]iridium(III), [Ir(Fppy)$_3$] (**11**); and tris(2-phenylpyridinato-C^2,*N*)iridium(III), [Ir(ppy)$_3$] (**12**)} representing red-, blue-, and green-emitting reference compounds, were characterized. The dyes were incorporated into standardized polystyrene films of 6 μm thickness. These were fabricated with a knife-coating device on a solid poly(ethylene terephthalate) (PET) support. The backside of the PET foil was coated with a highly reflective silicone/TiO_2 screen layer. The luminescence lifetimes were obtained according to the rapid lifetime determination (RLD) method.[29,30] This ratiometric method provides intrinsic referenced signals and can be used to calculate the average luminescence lifetimes. For this purpose, the sensor films were photoexcited by means of a pulsed 405 nm LED with an internal frequency of 125 kHz and 5 μs pulse lengths. The luminescence intensity was integrated by a triggered CCD camera within two precisely timed gates (A_1 and A_2) of 1.4 μs with delay times of 0 μs (t_1) and 0.7 μs (t_2) after the LED pulse, respectively. This was followed by the acquisition of the corresponding dark images for background subtraction. The whole imaging process has been described in previous work.[31]

The luminescence lifetimes (τ) can be calculated according to Equation (1),[32] when one assumes a monoexponential decay of luminescence emission, and with the two gates t_1 and t_2 being of the same width.

$$\tau = \frac{t_2 - t_1}{\ln A_1 / A_2} \quad (1)$$

The intrinsic referencing reduces the signal noise. It provides a highly reproducible signal, which is unsusceptible to the common interferences in luminescence measurements. It has to be emphasized that luminescence decays of metal–ligand complexes are not monoexponential, and the lifetimes determined by this simple ratiometric method do not represent exact values as obtained with single-photon counting measurements. However, the values acquired at identical experimental settings reflect changes of luminescence lifetimes within a series of measurements. For comparison, Baranoff et al. reported a lifetime τ_0 of the triplet emission of [Ir(btpy)$_3$] at 596 nm of 4.0 μs in toluene at 298 K[33] (see Table 4). Furthermore, the oxidation potential of the complexes was measured by means of cyclic voltammetry against ferrocene (Fc/Fc^+) in dried tetrahydrofuran. All determined parameters are summarized in Tables 4 and 5.

Table 4. Reversible oxidation potentials, phosphorescence emission maxima, and lifetimes of cyclometalated iridium(III) complexes and their pressure and temperature sensitivities.

	8b	**8c**	**10**	**11**	**12**
E_{ox} vs. Fc/Fc^+ [V]	0.27	0.28	0.25	0.64	0.31
Emission max. [nm]	590	521	596, (645)	470	512
τ [μs][a]	3.4	1.3	6.6	1.0	1.2
T coeff. [%(t)/°C]	0.43	0.48	0.35	0.31	0.19
K_{sv} [10^{-4} mbar^{-1}][b]	1.49	0.65	2.17	0.40	0.47

[a] At 50 mbar air pressure and 30 °C. [b] Stern–Volmer constant in 6 μm polystyrene (PS) film.

Table 5. Characterization of heteroleptic (phenylpyridine)-, (naphthylpyridine)-, and (phenylisoquinoline)iridium complexes with different ancillary ligands.

	7a	7b	7c	8b	8c	9b	9c
E_{ox} vs. Fc/Fc^+ [V]	0.26	0.27	0.25	0.27	0.28	0.27	0.27
Emission max. [nm]	625	600	526	590	521	595	522
τ [μs][a]	1.1	3.6	1.2	3.4	1.3	3.3	1.1
T coeff. [%(t)/°C]	0.21	0.40	0.37	0.43	0.48	0.40	0.43
K_{sv} [10^{-4} $mbar^{-1}$][b]	0.61	1.33	0.732	1.49	0.65	1.26	0.63

[a] At 50 mbar air pressure and 30 °C. [b] In 6 μm PS film.

In this study, the pressure and temperature calibration of the iridium(III) phosphors was performed with square samples of 3 × 3 cm size of the dyed PS films. These were placed in a calibration chamber, in which the air pressure can be adjusted from 50 to 2000 mbar and the temperature from 1 to 60 °C. The assembly of the calibration chamber and of the imaging set up has been outlined in a recent publication.[8] The results of the temperature calibrations are shown in Figure 6. The resulting lifetimes were normalized to the first value (1 °C at 1000 mbar) of the series of measurements to display the graphs in one plot. The results of the pressure calibrations are shown in Figure 7 in the form of Stern–Volmer plots. From the obtained data the Stern–Volmer (K_{SV}) constants and the temperature coefficients were calculated according to linear fits. The fits are very consistent in case of pressure dependency with correlation coefficients R^2 larger than 0.99. Although the temperature plots are apparently not linear, the calculated linear temperature coefficients are a suitable quantity for the temperature sensitivity.

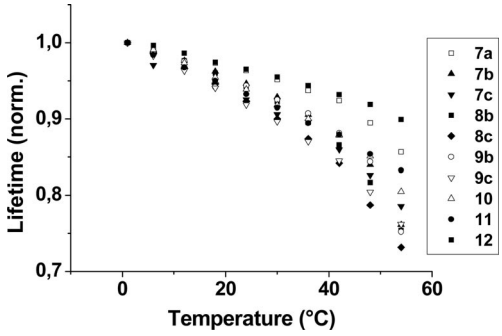

Figure 6. Temperature dependence of the normalized luminescence lifetimes of cyclometalated iridium(III) complexes **7**–**12** in 6 μm PS films at 1000 mbar.

Generally, in the cases of metal–ligand complexes, the emission maximum is determined by the energy gap between the excited triplet state and the ground state, which can be correlated with the energy difference of the frontier molecular orbitals (HOMO–LUMO gap). It is clear that increased HOMO–LUMO gaps result in emission maxima of higher energy. The oxidation potential, which depends on the energy level of the HOMO, decreases with lower energy gaps (see Table 4). Unfortunately, reduction potentials could not be measured with our setup. They occur at potentials lower than –2.0 V.[32]

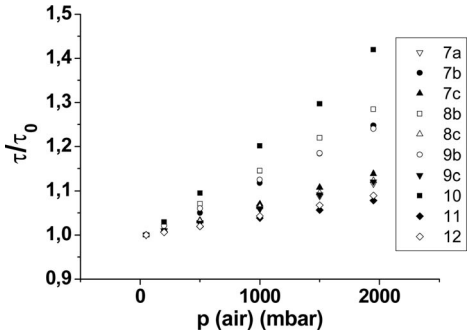

Figure 7. Air-pressure dependence of the luminescence lifetimes of cyclometalated iridium(III) complexes in 6 μm PS films at T = 30 °C. All plots are referenced to the according lifetime values at 50 mbar air pressure and 1 °C.

The influence of the ancillary ligand on the temperature and oxygen sensitivity is very small. Within a series of complexes that bear the same cyclometalating ligand (**7b**–**9b** or **7c**–**9c**, respectively) K_{SV} and temperature coefficients show only negligible deviations. In contrast, the cyclometalating ligands have a high impact on the sensing properties, as expected from their very different photophysical properties.

Calibration of Pressure Sensitivity

The series of homoleptic and heteroleptic Ir^{III} complexes that emit from blue to red also showed an increase in oxygen (and pressure) sensitivity with increasing lifetimes of the excited triplet state. This can be expected as a consequence of the Stern–Volmer equation [Equation (2)], which describes the dependency of the luminescence lifetime from partial oxygen pressure:

$$\frac{I_0}{I} = \frac{\tau_0}{\tau} = 1 + K_{SV}[Q] \quad (2)$$

in which I_0 is the luminescence intensity and τ_0 the lifetime in absence of quencher (oxygen) under standard conditions. I and τ are intensity and lifetime in the presence of oxygen with concentration [Q]. The presence of oxygen quenches the luminescence lifetime and intensity likewise.

K_{SV} is the Stern–Volmer constant defined in Equation (3), with K_q being the bimolecular dynamic quenching constant.

$$K_{SV} = \tau_0 \cdot K_q \quad (3)$$

The red-emitting series with the npy ligand (**7b**–**9b**) shows much higher oxygen sensitivity relative to the green-emitting series with the ppy cyclometalating ligand (**7c**–**9c**). With respect to Equation (3), this is due to the longer lifetimes of the complexes with the npy ligand. The highest oxygen-quenching efficiency is observed for $[Ir(btpy)_3]$ (**10**) with a K_{SV} of 2.17 [10^{-4} $mbar^{-1}$] relative to air pressure. Stern–Volmer constants of several cyclometalated iridium(III) complexes have been reported, but they can be hardly compared, because they have been determined under different experimental conditions and with various polymer

matrices.[16,34–39] Generally, with the exception of **10** and the npy complexes, the iridium(III) complexes are not very efficiently quenched by oxygen.

A general influence of the emission wavelength on the sensitivity to oxygen cannot be deduced as the deep red-emitting complex **7a** shows only slight oxygen sensitivity. It is apparent that the luminescence quenching by oxygen is a bimolecular process and is affected by many factors.

Another very important aspect that determines the response is the oxygen permeability of the matrix polymer. In this study, all complexes were calibrated in PS, which possesses an oxygen permeability P of 1.9×10^{-13} cm^3 (STP) cm (cm^2 s Pa)$^{-1}$ {the permeability coefficient P is defined by: P = [(quantity of oxygen)×(film thickness)]/[(area)×(time)-×(pressure drop across film)]} (STP = standard temperature and pressure).[40] Because of this moderate permeability, PS is an appropriate polymer binder to compare the luminescence responses to temperature and oxygen of a series of dyes under standard conditions. If polymers with higher oxygen permeabilities are applied, the oxygen sensitivity and K_{SV} values increase, and also the differences between the single complexes are more pronounced. Figure 8 compares the response to oxygen of complex **10** in PS and ethyl cellulose (EC). The latter provides a very high oxygen permeability with $P = 11 \times 10^{-13}$ cm^3 (STP) cm (cm^2 s Pa)$^{-1}$.[40] This results in an increased K_{SV} of 40 [10^{-4} mbar^{-1}], which is a very high sensitivity compared to other luminescent probes used in optical oxygen sensors. A comparison of the performance of [Ir(btpy)$_3$] as indicator for oxygen (or barometric pressure) with established oxygen-sensitive probes can be found in previous work.[16]

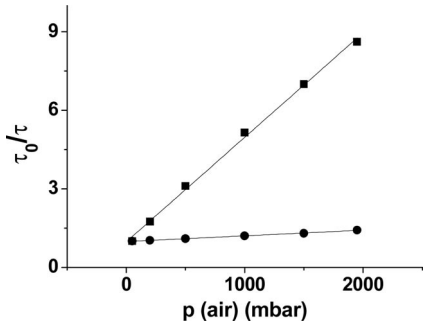

Figure 8. Stern–Volmer plots for **10** in PS (●) and EC 49 (▬) (EC with 49% ethoxy grade) at 30 °C.

Calibration of Temperature Sensitivity

Nearly all luminescent dyes display a strong sensitivity towards temperature. The Boltzmann distribution is one factor for this phenomenon, because it governs the populations of the different vibrational levels of the electronic states involved. The matrix polymer also influences the temperature dependency of the luminescence intensity. Generally, thermal quenching can be observed. This implies decreasing photoluminescence intensities and lifetimes with increasing temperature. Besides the factors discussed above, nonradiative relaxation mechanisms become dominant at higher temperatures, because deactivating states are thermally activated. For example, the decreasing energy difference between the electronic states can be converted more easily to vibrational energy in the complex ligand or in the polymer matrix. Furthermore, the energy of the excited electronic state can be transferred to appropriate electronic states of the environment. Finally, the oxygen permeability of the matrix polymer increases with temperature. This results in a higher concentration of quenching oxygen molecules in the polymer binder at increased temperatures. Among the studied iridium(III) complexes, the green-emitting series that bears ppy ligands (**7c**–**9c**) show the highest temperature sensitivity. The calibration plots for the temperature response are nonlinear and can be fitted by an Arrhenius-type equation [Equation (4)]:[11]

$$\frac{1}{\tau} = k_0 + k_1 \cdot \exp\left(-\frac{\Delta E}{RT}\right) \quad (4)$$

in which τ is the lifetime, k_0 the temperature-independent decay rate for the deactivation of the excited state, k_1 the pre-exponential factor, ΔE the energy gap between the emitting level and an upper deactivating excited state, R the gas constant, and T the temperature in Kelvin. Figure 9 shows exemplary the Arrhenius fit of the thermal quenching of **8c** in PS at 1000 mbar air pressure with the fitting parameters: $k_0 = 0.76$ μs^{-1}, $k_1 = 19.5 \times 10^4$ μs^{-1}, and $\Delta E = 36.5$ kJ mol^{-1}. The correlation coefficient R^2 for the fit is 0.994.

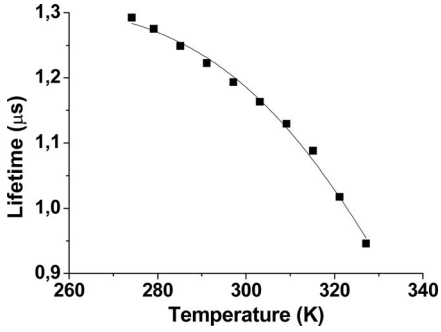

Figure 9. Temperature dependence of the luminescence lifetime of **8c** in PS at 1000 mbar and Arrhenius fit according to Equation (4) (straight line).

Generally, the temperature sensitivity of cyclometalated iridium(III) complexes is very low relative to other luminescent metal–ligand complexes. Hence, the temperature coefficients of typical luminescent indicators for T such as ruthenium and europium complexes[29,41,42] are up to two times higher than those of the green-emitting iridium(III) complexes described here. The exceptional property of the green emitters, particularly of **8c**, is their shortwave-emission wavelengths, which make them easy to combine with the numerously available red-emitting oxygen indicators for dual sensors. The high reproducibility and the very low standard deviations of the calibration plots and the broad dynamic range of the response are also advantageous.

Conclusion

The design of a full series of neutral heteroleptic iridium(III) complexes equipped with 2-phenylpyridine, 2-(naphthalen-1-yl)pyridine, and 1-phenylisoquinoline as cyclometalating ligands was presented. To obtain unsymmetrical iridium(III) complexes, 2,2,6,6-tetramethylheptane-3,5-dione, 1-(9*H*-carbazol-9-yl)-5,5-dimethylhexane-2,4-dione, and 1-[3,6-bis(4-hexylphenyl)-9*H*-carbazol-9-yl]-5,5-dimethylhexane-2,4-dione were utilized as ancillary ligands. These serve to gradually increase the unsymmetrical architecture of the Ir^{III} complexes. The photophysical and electrochemical properties of the Ir^{III} complexes were investigated experimentally as well as theoretically by extensive Δ-DFT and TD-DFT calculations on a selected set of Ir^{III} structures. Moreover, the properties of the carefully designed heteroleptic iridium(III) complexes were compared to homoleptic Ir^{III} complex structures that reveal symmetrical architectures. These consist of three equal cyclometalating ligands. The emission intensities of the two classes of heteroleptic Ir^{III} complexes respond to changes of partial oxygen pressure and, to a lesser extent, to temperature changes. Notably, oxygen-sensitive Ir^{III} emitters can be targeted due to the clear correlation of superior oxygen sensitivities with enhanced phosphorescence lifetimes.

Supporting Information (see footnote on the first page of this article): Experimental section of materials, instrumentation, calibration of pressure and temperature sensitivity, computational details, synthetic procedures, scheme for the synthesis of **2**–**5** (Figure S1), APLI-MS spectra, and references.

Acknowledgments

E. H., M. S., and O. S. acknowledge the Deutsche Forschungsgemeinschaft (DFG) for financial support. This research forms part of the research program of the Dutch Polymer Institute (DPI) (project no. 629). D. E. acknowledges the Carl-Zeiss Stiftung for financial support. We thank Dr. Ulrich Henne and Dr. Christian Klein from the German Aerospace Center (DLR) in Göttingen for providing the calibration unit and Ulrich Lange for his assistance in the electrochemical measurements. E. H. acknowledges Professor Ullrich Scherf for granting access to the tools of the Macromolecular Chemistry at the University of Wuppertal (BUW) and Anke Helfer for TGA analysis; Melanie Dausend and Jürgen Dönecke (Organic Chemistry, BUW) for performing routine mass spectrometry as well as Ralf Radon (Analytical Chemistry, BUW) for elemental analysis. Professor Otto S. Wolfbeis is acknowledged for helpful comments.

[1] K. Kalyanasundaram, M. Grätzel, *Coord. Chem. Rev.* **1977**, *77*, 347–414.
[2] A. J. Lees, *Chem. Rev.* **1987**, *87*, 711–743.
[3] S. Lamansky, P. Djurovich, D. Murphy, F. Abdel-Razzaq, R. Kwong, I. Tsyba, M. Bortz, B. Mui, R. Bau, M. E. Thompson, *Inorg. Chem.* **2001**, *40*, 1704–1711.
[4] S. Lamansky, P. Djurovich, D. Murphy, F. Abdel-Razzaq, H.-E. Lee, C. Adachi, P. E. Burrows, S. R. Forrest, M. E. Thompson, *J. Am. Chem. Soc.* **2001**, *123*, 4304–4312.
[5] H. Z. Xie, M. W. Liu, O. Y. Wang, X. H. Zhang, C. S. Lee, L. S. Hung, S. T. Lee, P. F. Teng, H. L. Kwong, H. Zheng, C. M. Che, *Adv. Mater.* **2001**, *13*, 1245–1248.
[6] C. Adachi, M. A. Baldo, M. E. Thompson, S. R. Forrest, *J. Appl. Phys.* **2001**, *90*, 5048–5051.
[7] E. Holder, B. M. W. Langeveld, U. S. Schubert, *Adv. Mater.* **2005**, *17*, 1109–1121.
[8] L. H. Fischer, M. I. J. Stich, O. S. Wolfbeis, N. Tian, E. Holder, M. Schäferling, *Chem. Eur. J.* **2009**, *15*, 10857–10863.
[9] Q. Zhao, M. Yu, L. Shi, S. Liu, C. Li, M. Shi, Z. Zhou, C. Huang F. Li, *Organometallics* **2010**, *29*, 1085–1091.
[10] K.-C. Tang, K. L. Liu, I.-C. Chen, *Chem. Phys. Lett.* **2004**, *386*, 437–441.
[11] J. N. Demas, B. A. DeGraff, *Anal. Chem.* **1991**, *63*, 829A–837A.
[12] Y. You, S. Y. Park, *Dalton Trans.* **2009**, 1267–1282.
[13] T. Sajoto, P. I. Djurovich, A. Tamayo, M. Yousufuddin, R. Bau, M. E. Thompson, R. J. Holmes, S. R. Forrest, *Inorg. Chem.* **2005**, *44*, 7992–8003.
[14] J. Qiao, L. Duan, L. Tang, L. He, L. Wang, Y. Qiu, *J. Mater. Chem.* **2009**, *19*, 6573–6580.
[15] H.-S. Duan, P.-T. Chou, C.-C. Hsu, J.-Y. Hung, Y. Chi, *Inorg. Chem.* **2009**, *48*, 6501–6508.
[16] C. S. K. Mak, D. Pentlehner, M. Stich, O. S. Wolfbeis, W. K. Chan, H. Yersin, *Chem. Mater.* **2009**, *21*, 2173–2175.
[17] M. C. DeRosa, D. J. Hodgson, G. D. Enright, B. Dawson, C. E. B. Evans, R. J. Crutchley, *J. Am. Chem. Soc.* **2004**, *126*, 7619–7626.
[18] L. Huynh, Z. Wang, J. Yang, V. Stoeva, A. Lough, I. Manners, M. A. Winnik, *Chem. Mater.* **2005**, *17*, 4765–4773.
[19] S.-J. Liu, Q. Zhao, Q.-L. Fan, W. Huang, *Eur. J. Inorg. Chem.* **2008**, 2177–2185.
[20] Y. Maegawa, Y. Goto, S. Inagaki, T. Shimada, *Tetrahedron Lett.* **2006**, *47*, 6957–6960.
[21] Y. Morisaki, J. A. Fernandes, N. Wada, Y. Chujo, *J. Polym. Sci., Part A: Polym. Chem.* **2009**, *47*, 4279–4288.
[22] M. Inoue, T. Suzuki, M. Nakada, *J. Am. Chem. Soc.* **2003**, *125*, 1140–1141.
[23] U. Jacquemard, S. Routier, A. Tatibouet, J. Kluza, W. Laine, C. Bal, C. Bailly, J.-Y. Merour, *Org. Biomol. Chem.* **2004**, *2*, 1476–1483.
[24] N. Tian, A. Thiessen, R. Schiewek, O. J. Schmitz, D. Hertel, K. Meerholz, E. Holder, *J. Org. Chem.* **2009**, *74*, 2718–2725.
[25] M. Nonoyama, *Bull. Chem. Soc. Jpn.* **1974**, *47*, 767–768.
[26] A. Dreuw, M. Head-Gordon, *Chem. Rev.* **2005**, *105*, 4009–4037.
[27] B. Beyer, C. Ulbricht, D. Escudero, C. Friebe, A. Winter, L. González, U. S. Schubert, *Organometallics* **2009**, *28*, 5478–5488.
[28] J. N. Demas, G. A. Crosby, *J. Phys. Chem.* **1971**, *75*, 991–1024.
[29] M. I. Stich, O. S. Wolfbeis, "Fluorescence Sensing and Imaging Using Pressure-Sensitive Paints and Temperature-Sensitive Paints" in *Standardization and Quality Assurance in Fluorescence Measurements I* (Ed.: U. Resch-Genger), *Springer Ser. Fluoresc.*, Springer Verlag Berlin Heidelberg, **2008**, vol 5, part E, 429–461.
[30] C. Moore, S. P. Chan, J. N. Demas, B. A. DeGraff, *Appl. Spectrosc.* **2004**, *58*, 603–607.
[31] G. Liebsch, I. Klimant, B. Frank, G. Holst, O. S. Wolfbeis, *Appl. Spectrosc.* **2000**, *54*, 548–559.
[32] J. H. Bell, E. T. Schairer, L. A. Hand, R. D. Mehta, *Annu. Rev. Fluid Mech.* **2001**, *33*, 155–206.
[33] E. Baranoff, J.-H. Yum, M. Graetzel, M. K. Nazeeruddin, *J. Organomet. Chem.* **2009**, *694*, 2661–2670.
[34] Y. Amaoa, Y. Ishikawa, I. Okura, *Anal. Chim. Acta* **2001**, *445*, 177–182.
[35] A. Medina-Castillo, J. Fernandez-Sanchez, C. Klein, M. K. Nazeeruddin, A. Segura-Carretero, A. Fernandez-Gutierrez, M. Graetzl, U. E. Spiqhiger-Keller, *Analyst* **2007**, *132*, 929–936.
[36] S. M. Borisov, I. Klimant, *Anal. Chem.* **2007**, *79*, 7501–7590.
[37] G. Di Marco, M. Lanza, M. Pieruccini, S. Campagna, *Adv. Mater.* **1996**, *8*, 576–580.

[38] G. Di Marco, M. Lanza, A. Mamo, I. Stefio, C. Di Pietro, G. Romero, S. Campagna, *Anal. Chem.* **1998**, *70*, 5019–5023.
[39] L. Huynh, J. Wang, V. Stoeva, A. Lough, I. Manners, M. A. Winnik, *Chem. Mater.* **2005**, *17*, 4765–4773.
[40] J. Brandrup, E. H. Immergut, E. A. Grulke, *Polymer Handbook*, Wiley-VCH, **1999**.
[41] M. E. Köse, B. F. Carroll, K. S. Schanze, *Langmuir* **2005**, *21*, 9121–9129.
[42] B. Zelelow, G. E. Kahlil, G. Phelan, B. Carlson, M. Gouterman, J. B. Callis, L. R. Dalton, *Sens. Actuators B* **2003**, *96*, 304–314.

Received: June 1, 2010
Published Online: August 26, 2010

